工學碩士 學位論文

Synthesis and characterization of a graphene oxide/polybenzimidazole nanocomposite membrane for water treatment

수처리용 그래핀 옥사이드/폴리벤지미다졸 복합막의 제조 및 분석.

2013年 7月

서울大學校 大學院

化學生物工學部

鄭 燦 昊

Synthesis and characterization of a graphene oxide/polybenzimidazole nanocomposite membrane for water treatment

指導敎授　李 鍾 贊

이 論文을 工學碩士 學位論文으로 提出함

2013年 6月

서울大學校 大學院

化學生物工學部

鄭 燦 昊

鄭 燦 昊의 工學碩士 學位論文을 認證함

2013年　6月

委 員 長 _____ (인)

副委員長 _____ (인)

委　　員 _____ (인)

Synthesis and characterization of a graphene oxide / polybenzimidazole nanocomposite membrane for water treatment

by

Chanho Jeong

June 2013

Thesis Adviser: Jong-Chan Lee

Abstract

Various approaches have been developed chlorine resistant membrane because PA membrane, which is currently the most widely used desalination process, suffurs from poor resistance to continual exposure to oxidizing agent such as chlorine. In this work, we studied the prospect of graphene oxide (GO) / polybenzimidazole (PBI) nano-composite (NF) membranes for water purification. PBI was chosen mainly because of its excellent chemical stability and the membranes show high chlorine resistance compared to the conventional polyamide membranes. To enhance the water flux and the salt rejection, GO was introduced in the PBI membrane. The reverse osmosis process involved semi-permeable thin film composite membranes with a sodium chloride feed solution. Fourier transform infrared spectroscopy (FTIR), X-ray photoelectron spectroscopy (XPS), contact angle, ζ potential, and water uptake were measured for membrane characterization. The composite membrane surface exhibit increased hydrophilicity and surface charge. Additionally, the membranes show increased water flux and a reduction in sodium chloride transport.

Keywords : desalination, polybenzimidazole, nano filteration membrane, nanocomposite membrane, graphene oxide, chlorine resistance

Student number: 2011-23415

TABLE OF CONTENTS

List of Figures

List of Tables

1. INTRODUCTION

An urgent need in the 21st century is access to secure, sustainable sources of fresh water [1]. Membrane-based desalination is an energy-efficient, low environmental impact route to produce clean water for a variety of applications. Capital, operation, and maintenance costs for membrane systems continue to decline, making them increasingly attractive for water purification applications [2]. Membrane separation processes, such as nanofiltration (NF) and reverse osmosis (RO), have developed rapidly over the last three decades into the dominant technology for desalination of water [3]. Commercially available RO membranes are derived from two basic classes of polymers: cellulose acetate (CA) and aromatic polyamides (PA). However, CA membranes are susceptible to microbiological attack, undergo compaction at higher temperatures and pressures, and are limited to a relatively narrow pH range [4]. On the other hand, PA membranes exhibit better transport properties at a given applied pressure and are more stable over a wider range of pH values than CA membranes [5]. Thus, PA thin-film composite membranes are currently the most widely used desalination membranes. However, PA membranes suffer from poor resistance to

continual exposure to oxidizing agents such as chlorine [6]. Chlorine is the most widely used oxidizing biocide in water treatment because it is inexpensive and highly effective when present in water at levels of a few parts per million [7]. Disinfection of feed water to membrane desalination units is required to prevent biofilm growth on the membranes, which significantly degrades their performance.[8] However, PA membranes cannot tolerate continuous exposure to water containing more than a few parts per billion chlorine.[6, 9] Consequently, membrane manufacturers recommend that feed-water chlorine concentration to such membranes be limited to concentrations lower than 0.1 ppm. To meet these conflicting requirements, water to be purified is often chlorinated, to disinfect it and ultimately inhibit biofouling of the membranes, then dechlorinated before being fed to membrane desalination units. After passing through the membranes, the water is then rechlorinated before being sent to the distribution network [10]. Thus, the sensitivity of PA membranes to chorine leads to significant additional processing steps and, in turn, increased water purification costs [11]. We describe a new platform of highly chlorine-tolerant polymers for use as desalination membranes. Such materials could expand the processing window for using chlorine in conjunction with desalination membranes, remove costly process steps, such as dechlorination and rechlorinations, and yield significant increases in

membrane lifetime. The removal of processing steps, leading to process intensification, and increase in membrane lifetime could lower water desalination costs. PBI is a polymer that exhibits high mechanical strength, thermal stability, and chemical resistance [12]. PBI has much better chlorine resistance than aromatic polyamides because its main chain consists of aromatic rings and chemically strong bonds between carbon and nitrogen, so it does not have the amide linkages that are sensitive to attack by aqueous chlorine [13]. It has been reported that salt rejection of PBI membrane was found to be highly dependent on the solution pH [14,15]. pH values determine the phases and sizes of the ionic species, in addition to the surface charge characteristics of the PBI membrane. It was also shown through surface modification of the PBI membranes that the rejection of aqueous solutes is highly dependent on both the membrane pore size and electrostatic interaction between the solute and membrane. Analysis of PBI membranes in pressure driven systems with single electrolyte solution at various pH values showed a decrease in solute permeability with modification at neutral pH values, with increasingly higher rejection as the pH increased and the membranes took on higher surface charges [16–18]. In this study PBI TFC membrane also showed higher salt rejection during chlorine tolerance test with a feed solution containing 500 ppm chlorine as NaOCl. The feed was buffered to pH 9.5. So costly process

steps, such as dechlorination and rechlorinations, don't need to PBI membrane and membrane lifetime will increases significantly in comparison with polyamide membrane. Using the phase inversion technique, asymmetric PBI membranes were formed yielding high water fluxes but low monovalent salt rejection in earlier studies [14,15]. In an attempt to enhance the salt rejection of the PBI membranes, we fabricated dense membrane by using the solvent evaporation method. For improved water permeability, the PBI thin film composite membrane prepared from spin coating of PBI film on a AAO substrate. The active layer thickness was about 1 μm.

Recent studies have indicated that improvements in wetting of a membrane surface can be critical in improving the membranes water permeability [19]. Significant drawbacks of PBI that prevent its use as a membrane for water purification applications include hydrophobicity and neutral surface charge at neutral pH values. Lack of sufficient wetting exacerbates internal concentration polarization and disrupts continuity of water throughout the membrane structure. Decreased water continuity within the internal membrane pathways reduces the effective porosity, thus reducing water transport. This study [19] showed that water permeability could be increased due to the enhanced wetting effect, and subsequent removal of air and vapor trapped in the

porous selective layer of the membrane. Additionally, If the membrane surface is modified to be more hydrophilic, then the wetting effect of the membrane surface can be enhanced. To enhance wetting effect and hydrophilicity of membrane, GO was introduced in the PBI membrane. GO has both carboxyl (-COOH) and hydroxyl (-OH) functional groups that can either protonate or deprotonate based on the solution pH, and it is hydrophilic in nature [20,21]. The addition of GOs increases free volume of the composite membranes as a result of the weak interaction between GO and PBI matrix suggesting a incompact structure with increased membrane surface charge and wettability.

2. EXPERIMENTAL

2.1. Materials

Isophthalic acid (99 %) was purchased from Aldrich and purified by recrystallization in ethanol to obtain white needle-like products. 3,3-Diaminobenzidine tetrahydrochloride dihydrate (DABIT) was prepared by adding 3,3-diaminobenzidine (97 %, Tokyo Kasei TCI) to hydrochloric acid solution and recrystallized from water and hydrochloric acid as brown needles. Phosphorous pentoxide (97 %, Aldrich), polyphosphoric acid (116 % H_3PO_4, Junsei), and other solvents were used as received. All the monomers were dried under vacuum at 60 °C for 2 days before use. A commercially available AAO membrane filter template (Whatman, Anodisc, 0.02 micrometer pore), consisting of nanopores containing nanoscale spikes within microscale undulation on the surface and having a surface roughness of 14.7 nm, was used as the support membrane. $NaNO_3$(99 %, Aldrich), H_2SO_4(95 %, Aldrich), $KMnO_4$(99 %, Aldrich), H_2O_2(30 %, Daejung) were used as received. Graphite flakes (average paricle diameter of 20 mm, 99.5 % purity, BASF Korea Co., Ulsan, Korea) were oxidized using modified Hummers method. SWC5-LD (Hydranautics a Nitto

Denko, Oceanside, CA, USA) was used as a representative polyamide RO membrane since it is well characterized and widely used in seawater desalination. Membranes were cut into flat sheets and preserved with deionized water at 4 °C prior to the experiments.

2.2. Synthesis of polybenzimidazole

Poly[2,2'-(m-phenylene)-5,5'-bibenzimidazole] (PBI) was synthesized by condensation polymerization of DABIT with isophthalic acid [22], respectively, with a molar ratio of 1:1 in polyphosphoric acid (PPA) as shown in Fig. 1. A 250mL three-neck reactor equipped with a mechanical stirrer, a nitrogen inlet and a calcium chloride drying tube was charged with PPA, and then heated to 150 ℃. Purified DABIT (5.139 g, 12.97 mmol) was added gradually to this reactor, and then the solution was stirred for 4 h at 150 ℃ to remove hydrogen chloride from the DABIT under a slow stream of nitrogen. 12.97 mmol (2.155 g) of isophthalic acid was added to this solution. This mixture was heated to 240 ℃ then stirred for 30 min. 51.11 mmol (7.254 g) of phosphorous pentoxide was added and heating was continued at 240 ℃ for 12 h. PPA (67 g) were used for the preparation of 5 wt.% of PBI solutions, respectively. These polymer concentrations were calculated by a comparison of the estimated amounts of the resulting polymers (generated from the condensation reaction of monomers) and PPA solution (initial PPA amount and the amount of phosphorous pentoxide and water eliminated during the polymerization). When PPA (87 g) was employed to prepare 4 wt.% of polymer concentration, the resulting polymer precipitated during the polymerization process [23]. The rest

of the polymerization solution was poured into distilled water (800 mL) and the precipitate was washed several times with distilled water to remove PPA. The polymer was powdered by a pulverizer (A11 basic, IKA) and any remaining phosphoric acid in the polymer powder was further removed by extraction with distilled water in a Soxhlet extractor. Finally, the powder product was dried at 70 ℃ under vacuum for 3 days.

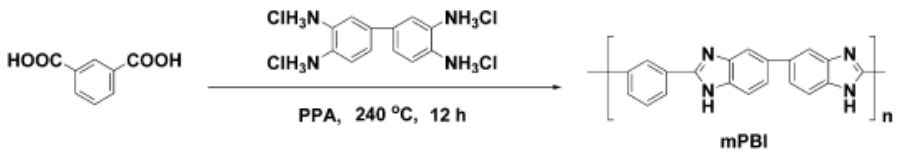

Fig. 1. Scheme of synthetic route for production of poly[2,2'-(m-phenylene)-5,5'-bibenzimidazole] (PBI).

2.3. Synthesis of graphite oxides

The GO was prepared using modified Hummers method [24] from flake graphite as shown in Fig. 2. Briefly, 10 g of graphite and 7.5 g of $NaNO_3$ were placed in a flask. Then, 750 mL of H_2SO_4 was added with stirring in an ice water bath, and 45 g of $KMnO_4$ were slowly added over about 1 h. Stirring was continued for 2h in the ice-water bath and 5 days at room temperature. Another 22.5 g of $KMnO_4$ was slowly added and stirring was continued for 2 h in the ice-water bath and another 5 days at room temperature. Then the same procedure was repeated twice more. 1400 mL of 5 wt.% H_2SO_4 aqueous solution was added over about 1 h with stirring, and the temperature was kept at 98 ℃. The resultant mixture was further stirred for 2 h at 98 ℃. The temperature was reduced to 60 ℃, 30 mL of H_2O_2 was added, and the mixture was stirred for 2 h at room temperature. To remove the ions of oxidant and other inorganic impurity, the resultant mixture was purified by repeating the following procedure cycle 15 times: centrifugation, removal of the supernatant liquid, addition of 2 L of a mixed aqueous solution of 3 wt % H_2SO_4/0.5 wt % H_2O_2 to the bottom solid, and dispersing the solid using vigorous stirring and bath ultrasonication for 30 min at a power of 140 W. Then a similar procedure was repeated: three times using 3 wt % HCl aqueous solution (2 L) and one time

using H_2O (2 L). Water was then removed to obtain the desired GO products [25].

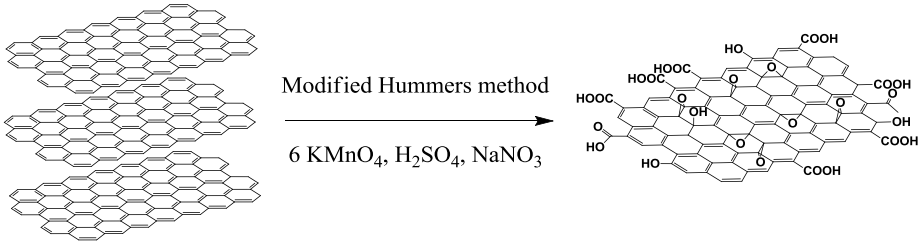

Fig. 2. Preparation of graphene oxide.

2.4. Fabrication of GO/PBI composite membranes

The properties of the synthesized composite membranes were compared with those of membrane controls cast from solutions containing PBI concentrations from 2 % to 6 %. A homogeneous PBI solution was obtained by dissolving the polymer in DMAc solution containing 2 wt.% LiCl. LiCl was a stabilizer of PBI/DMAc solution. the mixture was heated with stirring for 12 h at 80 ℃ and further filtered through a sintered glass filter (Duran, pore size 50 μm). The inherent viscosity of PBI was 2.45 dL g^{-1} [22]. The PBI solution was coated on a AAO membrane filter template (Whatman, Anodisc, 0.02 micrometer pore) using a spin coater (Laurell model WS-400A-6NPP/LITE). The AAO filter were dipped in DMAc for 5 min, placed on silicon wafer and spin coated with PBI / DMAc solution (5 s at 500 rpm then 600 s at 2000 rpm) to form a uniform thin film. A selective layer thickness of 1 μm was obtained by controlling the amount of casting solution. The solvent was evaporated slowly at 50 ℃ for 12 h under a ventilated hood and then dried at 70 ℃ under vacuum for 2 days. When the solvent was completely evaporated, cooling to room temperature, the resulting brown coloured film was cooled and immersed in deionized water bath for 24 h at room temperature to remove LiCl. For the preparation of GO/PBI composite membrane,

GOs were dispersed in DMAc solvent via ultrasonication for 2 h. DMAc solvent was prepared with lithium chloride salts (2 % (wt./v)) as a casting solution for the PBI membranes [22]. This DMAc LiCl solution was prepared by adding 0.2 g of LiCl to 10 mL of DMAC and heating to complete dissolution. Six different membranes were synthesized containing 0.1, 0.5, 1, 5, 10 and 50 mg GOs/g PBI, respectively with a constant PBI concentration of 4 wt.% by weight in the casting solution. All membranes were stored at ambient temperature under vacuum until testing and all experiments were performed under an atmosphere of N^2.

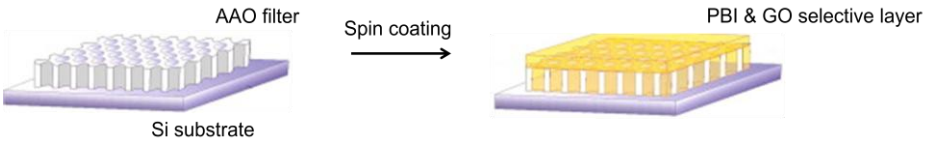

Fig. 3. Preparation of AAO-PBI thin film composite membrane.

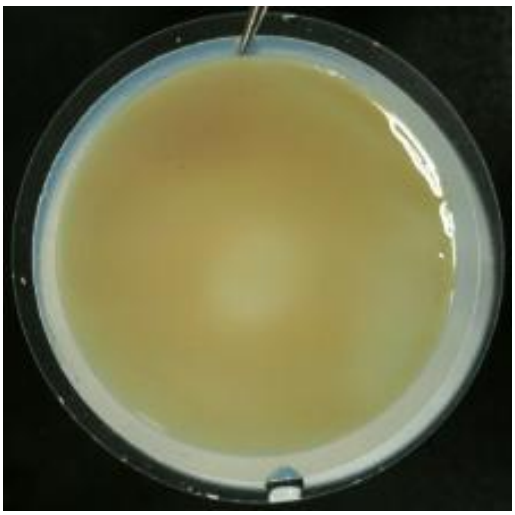

Fig. 4. Digital photo of the PBI coated on an AAO disk.

2.5. Characterization of GO/PBI composite membrane

A general characterizations of the graphite oxide product and GO/PBI composite membrane were carried out by means of X-ray photoelectron spectroscopy (XPS) and Fourier transform infrared (FTIR) spectroscopy. XPS spectra were recorded on an AXIS-HSi spectrometer (KRTOS) with an Al Kα radiation (1486.6 eV). FTIR spectra were recorded with a Nicolet 6700 spectrometer (Thermo Scientific, USA) using pellets in KBr with a sample concentration of ~0.1 wt.%. The recorded spectra were the result of coadding 64 interferograms obtained at a resolution of 4 cm^{-1}. The surface topology of the GO sheet was measured by non-contact mode AFM (SPA 400 with a SPI 3800 controller, Seiko Instruments Industry, Co. Ltd., Japan) using a silicon nitride cantilever (NCH Point Probe, Nanoworld, Neuch_tel, Switzerland) with a resonance frequency of 320 kHz and a spring constant of 42 Nm^{-1}. Samples for AFM images were prepared by depositing a dispersion of GO/H_2O solution (0.1 mg ml^{-1}) on a freshly cleaved mica surface and allowing them to dry in air.

Inherent viscosity of PBI were measured by means of an Ubbelode viscometer in a water bath at 30 ℃. 0.125 g of a polymer dried under vacuum at 70 ℃ for 2 days was placed in a 25mL volumetric flask and dissolved in 96 % H_2SO_4 (concentration 0.5 g dL^{-1}).

Characterizations of functional groups on the pristine PBI membrane and GO/PBI composite membranes was done by Fourier transform infrared (FTIR) spectroscopy (Nicolet 6700, ThermoScientific, USA) using films about 10 μm thick. Membrane samples were rinsed with deionized water and then dried in a vacuum oven before analysis. IR spectra of the membranes were recorded in transmittance mode over a wave number range of 4000 to 650 cm^{-1} at 25 ℃.

The surface morphology of the membrane was investigated by scanning electron microscopy (SEM) (JSM-6701F, JEOL co., Tokyo, Japan). The advancing and receding contact angles of deionized water were measured at room temperature and ambient relative humidity using a contact angle analyzer (Krüss DSA 10, Hamburg, Germany) interfaced to drop shape analysis software. The advancing contact angle was measured by supplying (and retreating in the case of measuring the receding contact angle) a liquid onto the polymer surface at the slowest possible rate using a motorized syringe device, and the contact angles were adopted in the region of the equilibrium state showing a constant contact angle. The contact angles for each sample were measured more than six times on three independently prepared films, and the values were averaged. The standard deviations were within 1.58 for all samples. The water uptake of PBI and, as a comparison, GO/PBI

composite membranes was investigated. The measurements were performed on well-hydrated membrane samples immersed in distilled water at least for 4–5 days. Then the samples were taken out of the liquid, blotted with filter paper and weighed. After the weight and dimension were measured, the membranes were dried under vacuum at 110 ℃. During drying, the weight and dimension changes were measured for a period of up to 140 h. Streaming zeta potentials, a measure of surface charge, of membranes were measured using an electrophortic light scattering spectrophotometer (ELS-8000, Otsuka Electronics Co., Hirakata, Japan). Before the test, membranes were rinsed with copious amounts of DI water. The KCl electrolyte solution used in these measurements had an ionic strength of 1.0 mM. The pH was adjusted using a 0.5 M NaOH solution [26].

2.6. Membrane permeability and rejection

Permeate flux and salt rejection were measured to test membrane separation performance. the membrane samples were operated in Dead end flow cell (HP 4750, Sterlitech, USA) with the feed solution. 1 mM NaCl aqueous solution was used as feed and the test experiments were performed at pH 7 and room temperature. Measurements of permeate volume were taken at intervals of 15 min for 1 h and at a single constant operating pressure (225 psi) under stirred conditions. The concentrations of electrolyte (NaCl) in the feed and permeate over time were measured using a standardized digital pH/conductivity meter (Inolab cond 730P, WTW Co., Germany).

2.7. Chlorine tolerance

Characterizations of functional groups on the PBI membrane and PA TFC membranes (SWC5) was done by Fourier transform infrared (FTIR) spectroscopy (Nicolet 6700, ThermoScientific, USA). Membrane samples were exposed by a feed solution containing 1mM NaCl and 500 ppm chlorine as NaOCl; the feed was buffered to pH 9.5. After 24 h, Membrane samples were rinsed with deionized water and then dried in a vacuum oven before analysis. IR spectra of the membranes were recorded in transmittance mode over a wave number

range of 4000 to 650 cm^{-1} at 25 ℃.

After PBI membrane and PA TFC membrane were exposed by the feed solution, the membrane samples were operated in Dead end flow cell (HP 4750, Sterlitech, USA) with the feed solution. NaCl rejection and permeate flux was presented as a function of chlorine exposure time. The sample was prepared from 4 wt.% PBI solution. A commercial RO membrane (SWC5, Nitto Denko Hydranautics) was run for comparison.

3. RESULTS AND DISCUSSION

3.1. Characterization of polybenzimidazole

3.1.1. Fourier transform infrared (FTIR) spectroscopy

Poly[2,2'-(m-phenylene)-5,5'-bibenzimidazole] (mPBI) was synthesized from DABIT and IPA via condensation polymerization in PPA. The formation of PBI was identified by FT-IR spectra as shown in Fig. 2. Polymer showed characteristic absorption bands at 3450-3250 and 1640 cm^{-1}, which were assigned to the stretching vibration of the N–H groups and C=N groups in the imidazole units, respectively. The disappearance of C=O stretching vibration at 1780-1650 cm^{-1}, suggesting the nearly complete closure of the imidazole rings [27,28]. A small shoulder at 3063 cm^{-1} from the stretching modes of the aromatic C–H groups and a small peak at 1527 cm^{-1} from the ring vibration characteristic of conjugation between benzene and imidazole rings, respectively, are also detected. The presence of benzimidazole group was, in addition, confirmed by characteristic bands at 1445 cm^{-1} due to the in plane deformation of benzimidazole rings and additional peaks were showed at 806 and 700 cm^{-1} assigned to the C–H out of plane deformation vibrations..

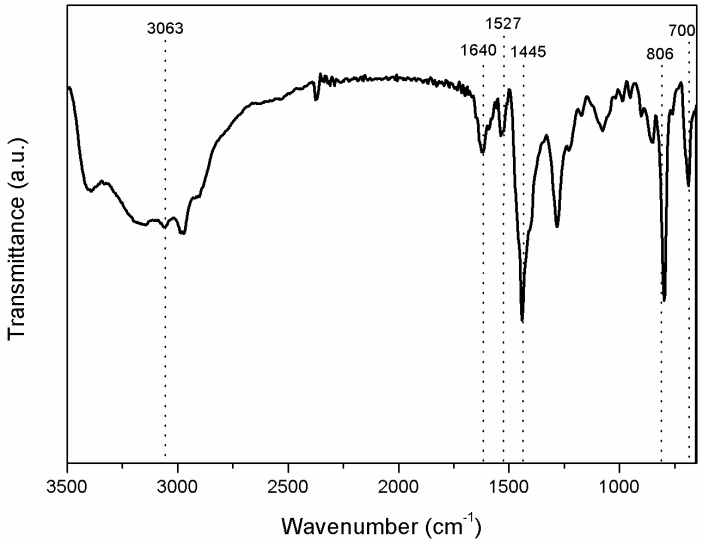

Fig. 5. FT-IR spectral analysis of the PBI.

3.2. Characterization of GO

3.2.1. X-ray photoelectron spectroscopy

The degree of oxidation of graphite oxide was confirmed by XPS. spectra of Cls level are plotted in Figure 6. An asymmetric photo-electron peak is observed, which can be deconvoluted in three peaks at 284.5, 286.5 and 287.6 eV for the oxidized samples (GO). The first two are more intense than that at 287.6 eV, and they have been previously assigned to C-C bonds in aromatic networks such as graphite, and to C-O bonds in alcohols or phenols[29-32]. The third peak, located at 287.6 eV, can be assigned to carbonate or CO_2 according to Desimoni et aL[31,33]. All these results point out that pristine graphite is slightly oxidized by atmospheric oxygen and exhibits the typical graphite structure with the characteristic graphite peak at 284.5 eV. After oxidation reaction, the intensity of the peak at 286.5 eV, owing to C-O single bonds, increases.

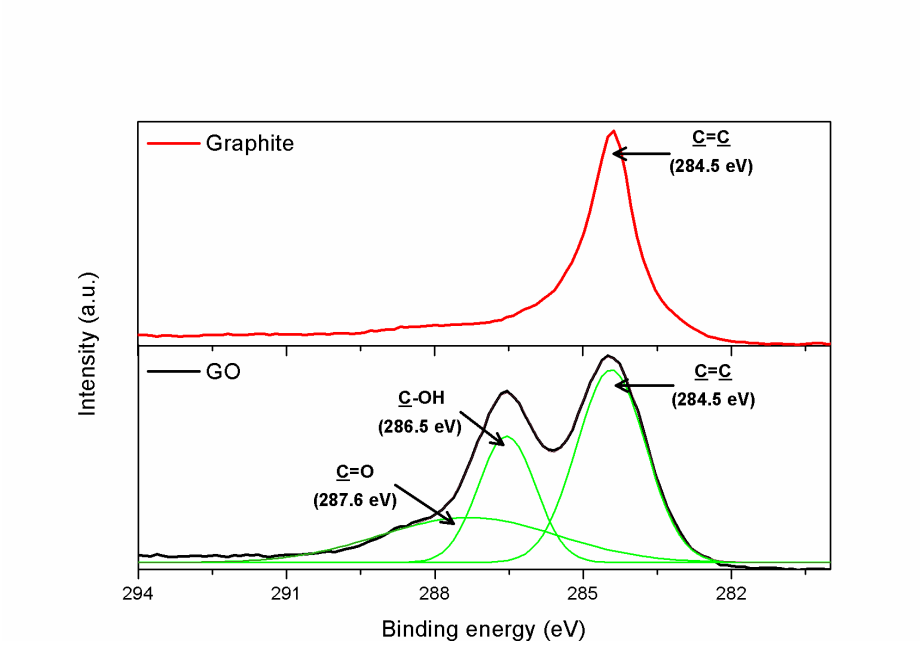

Fig. 6. High-resolution core-level C 1s XPS spectra for graphite and graphite oxide (GO).

3.2.2. Fourier transform infrared spectroscopy (FTIR)

Figure 7 shows the typical FT-IR spectrum obtained for our graphite oxide material. The most characteristic features are the broad, intense band at 3430 cm^{-1} (O-H stretching vibrations) and the bands at 1726 cm^{-1} (C=O stretching vibrations from carbonyl and carboxylic groups), 1621 cm^{-1} (skeletal vibrations from unoxidized graphitic domains), 1226 cm^{-1} (C-OH stretching vibrations), and 1089 cm^{-1} (C-O stretching vibrations) [34-36]. Thus, similar to XPS, FTIR spectroscopy provided evidence of the presence of different types of oxygen functionalities on the graphite oxide material.

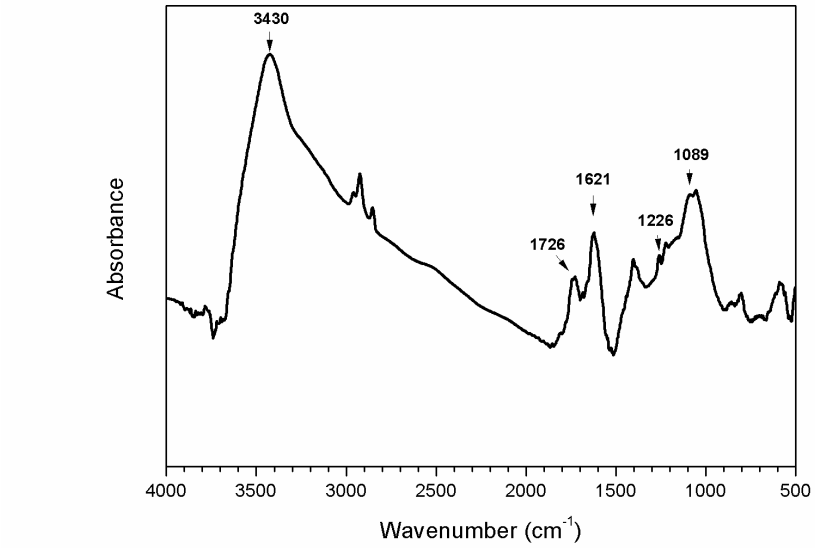

Fig. 7. FT-IR spectrum of graphene oxide.

3.2.3. Atomic force microscopy (AFM)

AFM measurements showed the complete exfoliation of GO (Fig. 8). After sonication for 1 h, the resulting GO particles were mostly single layered (topographic height ~1.0 nm) and 1~2 μm in lateral width according to atomic force microscopy (AFM) characterization.

(a)

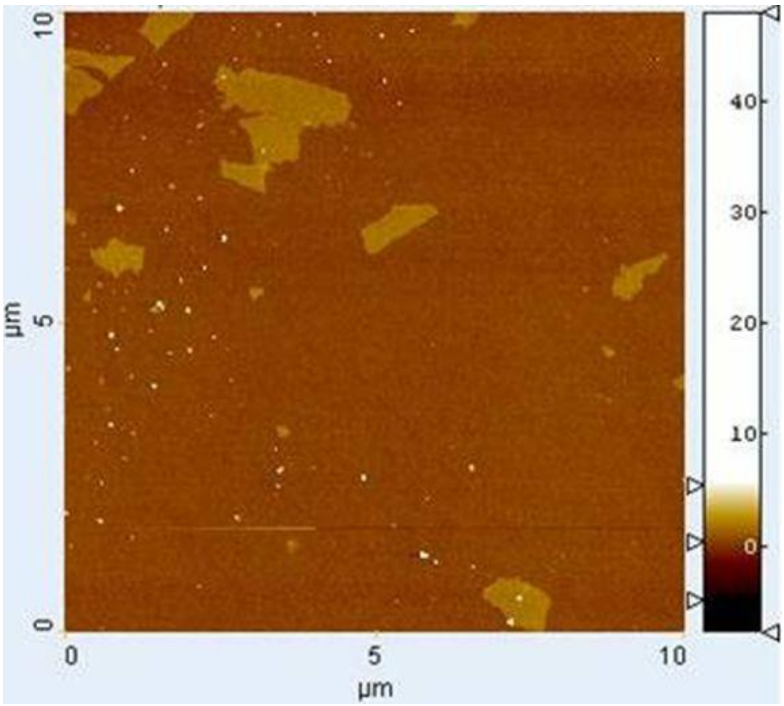

(b)

Fig. 8. (a) AFM image and (b) line profile of graphene oxide sheets deposited from dispersions in water onto a mica substrate.

3.3. Membrane characterization

3.3.1. Scanning electron microscopy (SEM)

The cross section SEM image (Fig. 9) for the PBI TFC membrane prepared from spin coating of PBI film on a AAO substrate showed a thin and flat laminar active layer. The active layer thickness was about 1 μm. Representative surface images of the composites with different GO loadings from 0 to 5 wt.% are shown in Fig. 11. SEM imagery of the functionalized graphene oxide in the resulting film showed GOs to be well mixed and evenly distributed throughout the polymer matrix at low concentration. While the surface of the PBI film is featureless, the composite film with 0.1 wt.% GO has a lot of GO sheets protruding out (Fig. 11d). While GO sheets are randomly distributed along the film surface, they are oriented aligned parallel to the film surface. However, an excessive filler concentration can cause the nanoparticles aggregation and make them not to disperse uniformly in polymeric matrix (Fig. 11g).

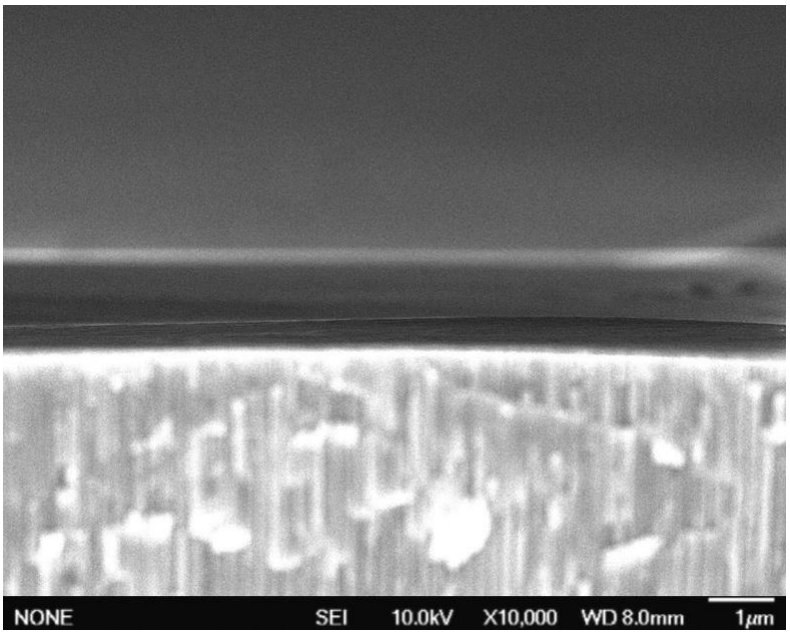

Fig. 9. SEM image (cross section) of the GO/PBI composite films on an AAO disk.

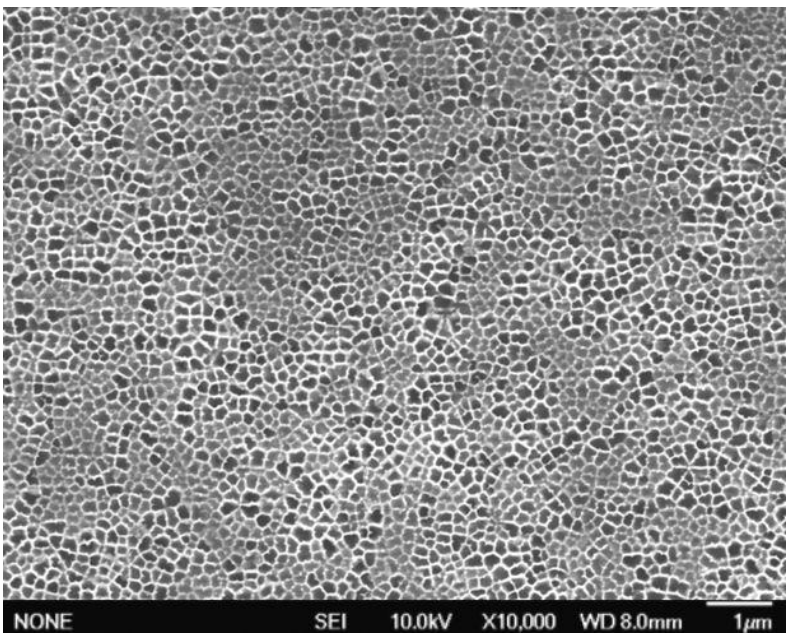

Fig. 10. SEM image (top view) of the bare AAO disk.

(a)

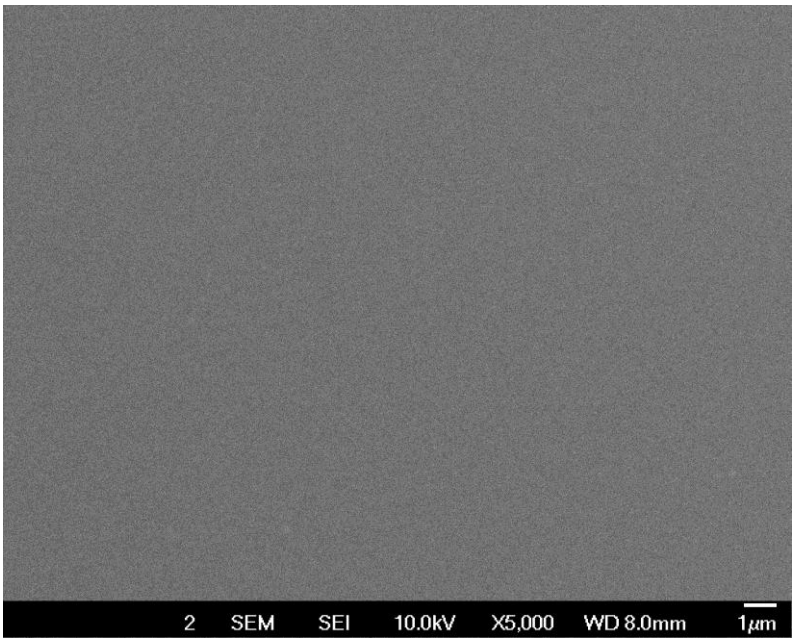

(b)

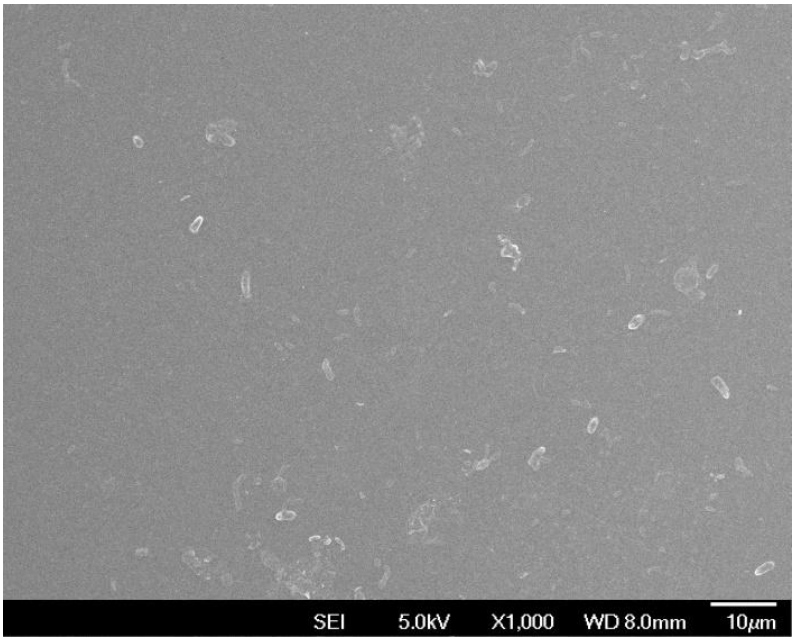

(c)

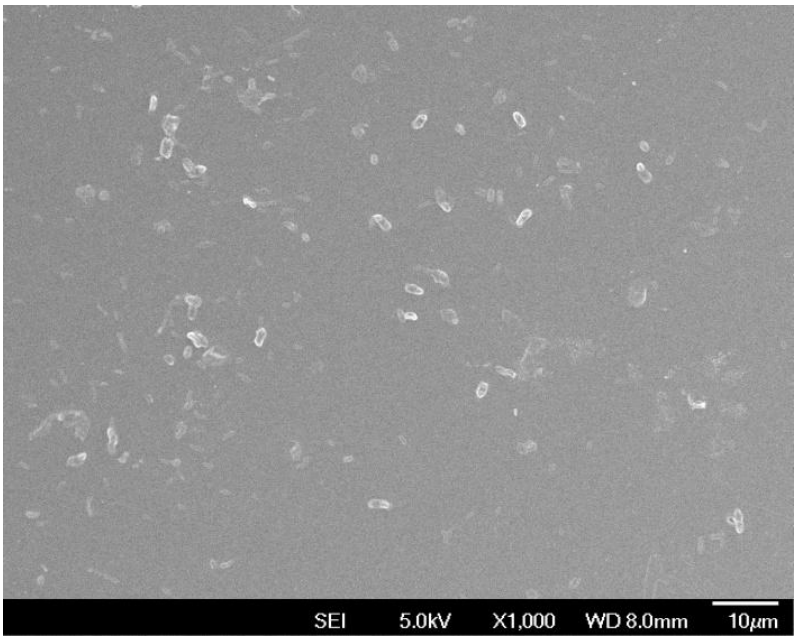

(d)

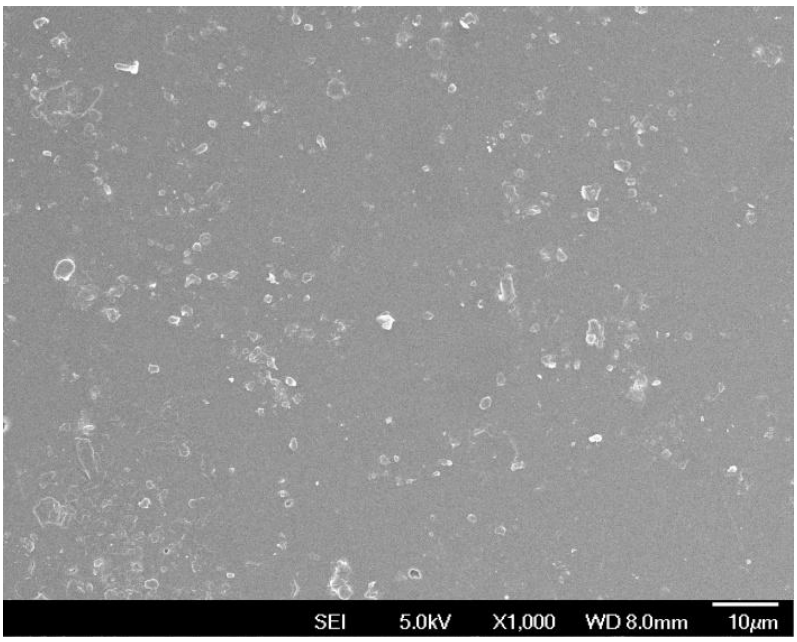

(e)

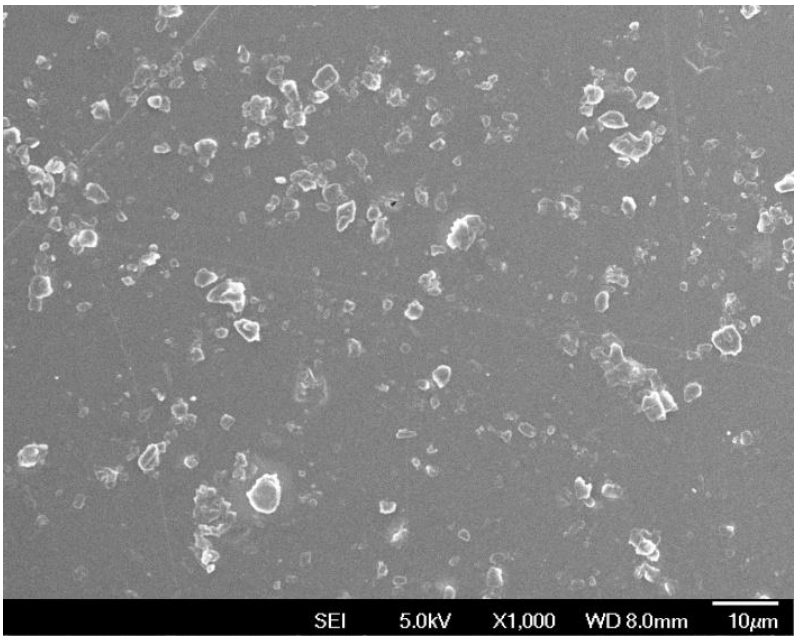

(f)

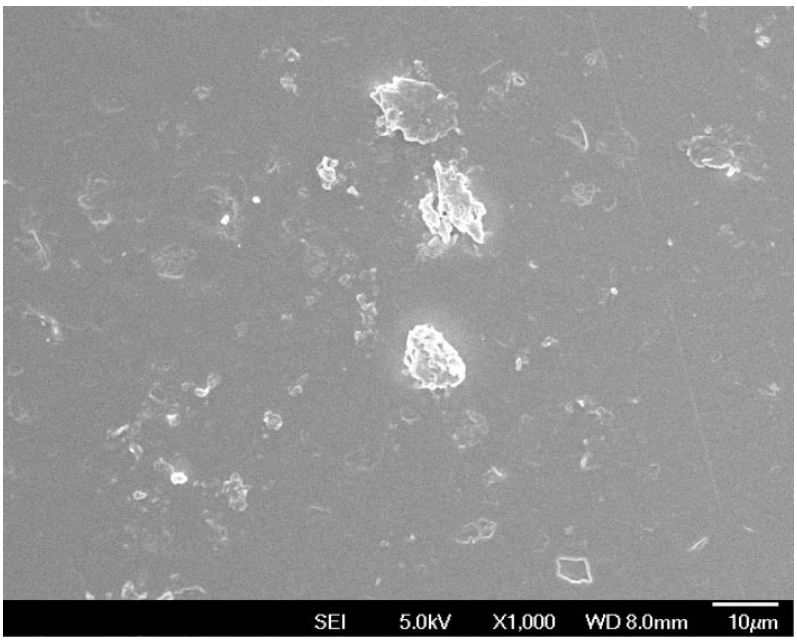

(g)

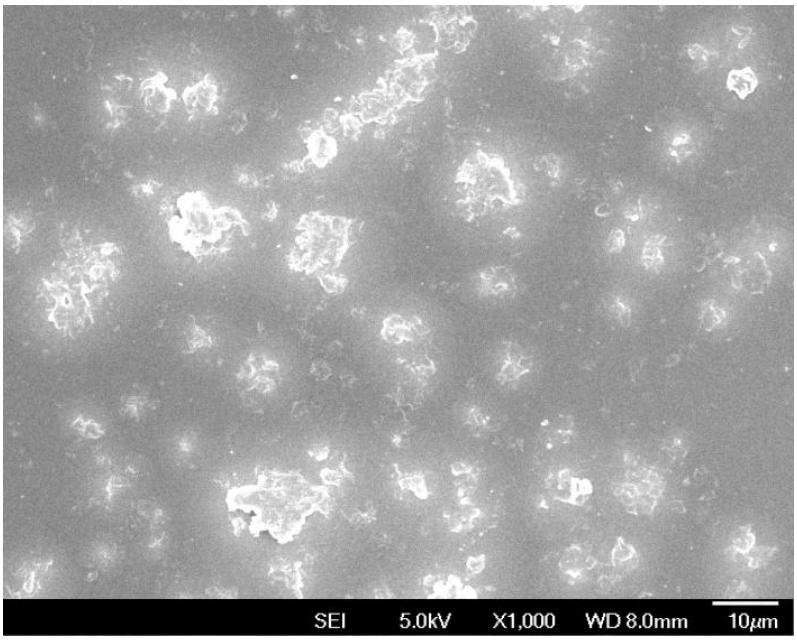

Fig. 11. SEM images (top view) of the GO/PBI composite films containing (a) 0 wt.%, (b) 0.01 wt.%, (c) 0.05 wt.%, (d) 0.1 wt.%, (e) 0.5 wt.%, (f) 1 wt.%, (g) 5 wt.% GO on an AAO disk.

3.3.2. Fourier transform infrared (FTIR) spectroscopy

Figure 12 shows the FT-IR spectra analysis of the pristine PBI membrane and PBI-GO composite membrane with contents of 5 wt.% GO. The FT-IR spectrum of the composite membrane is quite similar to the IR spectra of pristine PBI membranes and shows the absorption bands at 1089 cm^{-1} (alkoxy/alkoxide C-O) and 1726 cm^{-1} (carboxyl C=O) [34-36]. This is attributed to the presence of carboxylic acid group and hydroxyl group in the composite membrane.

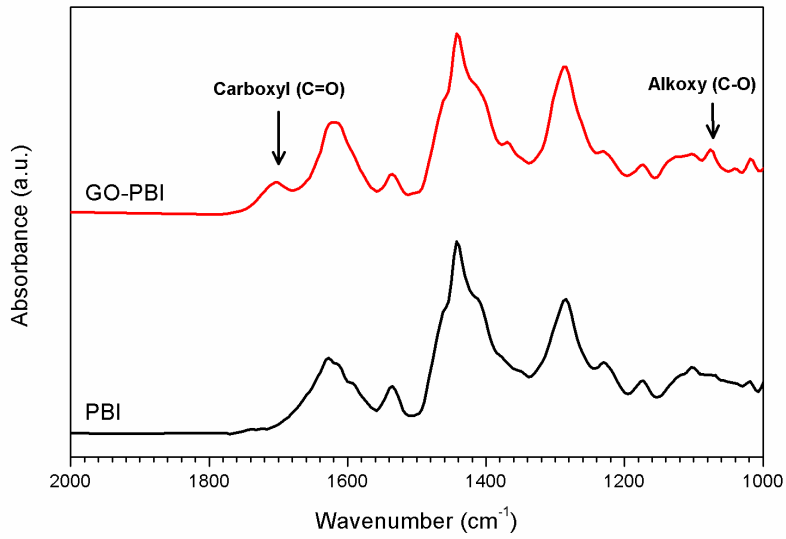

Fig. 12. FTIR absorption spectrum of PBI membrane and GO-PBI composite membrane. The range of wavenumber is from 2000 cm^{-1} to 1000 cm^{-1}.

3.3.3. X-ray photoelectron spectroscopy (XPS)

In constrast to pristine PBI membrane, the C1s XPS spectrum of GO-PBI composite membrane shows increased component for C from the hydroxyl group (286.5 eV) and carboxyl group (287.6 eV) [29-33], which is in agreement with the FT-IR results (Figure 13). All FT-IR and XPS spe-ctra would support the presence of carboxylic acid group and hydroxyl group in the composite membrane. FT-IR and XPS studies the presence of carboxylic acid group and hydroxyl group in the composite membrane. by dispersed GO.

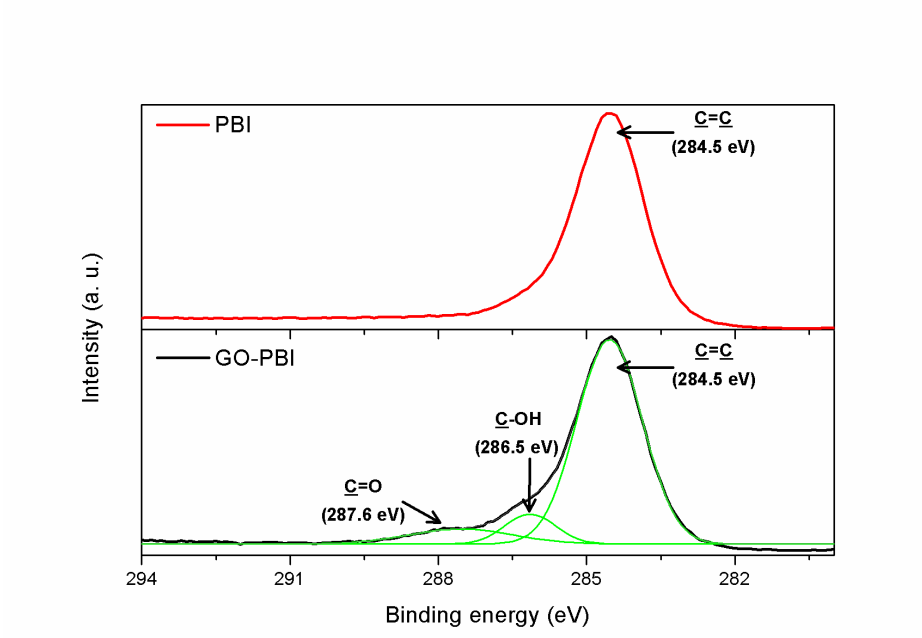

Fig. 13. Deconvoluted XPS spectrum of PBI and GO/PBI composite membrane in the C1s region.

3.3.4. Contact angle

Fig. 14 shows contact angle measurements for the pristine PBI membrane and GO/PBI composite membrane. The hydrophilicity of the surface increased after embedding GO in the PBI matrix as shown by decrease in contact angle, the 5 wt.% composite membrane were the most hydrophilic. This was most likely due to its greater ability to hydrogen bond and wettability. The increased hydrophilicity was most likely due to the carboxylic acid and hydroxyl groups associated with GO contains oxygen groups, which contain pairs of free electrons and also has the ability to hydrogen bond. The contact angle decreased from approximately 96° to 61° as the fraction of GO in the membrane increased from 0 to 5 wt.%. These results are consistent with the hydrophilic nature of graphene oxide. it is notable that such a significant difference in contact angle is produced at small concentrations of GO.

(a)

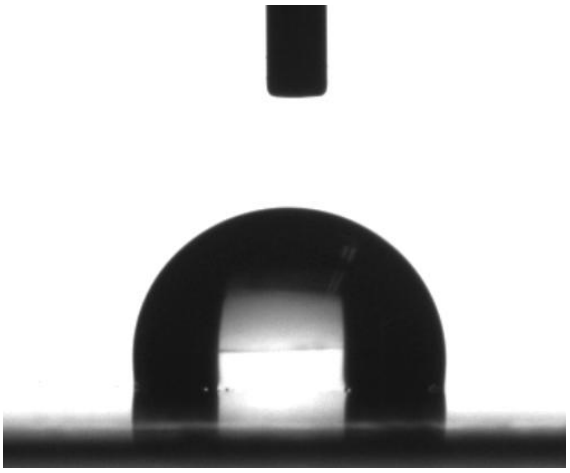

(b)

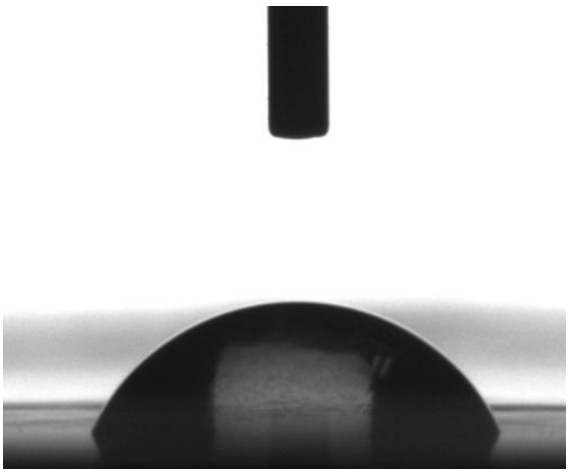

Fig. 14. Contact angle measurements for (a) the pristine PBI membrane and (b) GO/PBI composite membrane (5 wt.%). The contact angle decreased from approximately 96° to 61° as the fraction of GOs in the membrane increased.

3.3.5. ζ potential

The change in surface charge was detected using ζ potential as shown in Table 1. A net negative surface coverage was added to the surface of the membrane. Initially, the negative surface charge of the unmodified PBI membrane was 3.82 mV; that is, the membrane surface was mostly comprised of neutral and positive charges. This is consistent with one of the two key drawbacks of PBI membranes for desalination applications that they are not negatively charged at neutral pH value [14,15]. Embedding GO in PBI matrix led to an overall increase in the percentage of negative coverage of the composite membrane surfaces, as expected since GOs were chosen for their ability to impart negative charge to surfaces. The addition of GOs to the 4 wt.% PBI membrane increased negative charge from 3.82 to -17.5 mV as the GO loading increased from 0 wt.% to 5 wt.%. it shows that GO imparted more negative charges to the surface of PBI.

3.3.6. Water uptake

The water uptake of the pristine membrane and composite membranes were determined by measuring the changes in weight between the wet and dry membranes as shown in Table 1. It is well known that PBI has a high affinity for moisture and is hydrophilic. By immersing a PBI membrane in distilled water at room temperature, it was found that up to 24 wt.% of water (on basis of dry polymer, the same below), can be absorbed, corresponding to about 4 water molecules per repeat unit of benzimidazole. This water uptake seems to be rather high when compared with other engineering polymers, for example, polyimide (1.2 wt.%), polyetherketone (0.5 wt.%) and polycarbonate (0.3 wt.%) [37], and is supposed to be due to intermolecular hydrogen bonding between water and N and N–H groups in the PBI [38]. Additionally, the addition of GOs to the 4 wt.% PBI membrane increased water uptake from 24 % to 53 % as the GO loading increased from 0 wt.% to 5 wt.%. The addition of GO increases free volume of the composite membranes as a result of the weak interaction between GOs and PBI matrix suggesting a incompact structure with increased membrane hydrophilicity and wettability.

Table 1. Summary of contact angle, ζ potential, water uptake as a function of different GOs loadings.

GOs loading (wt.%)	Contact angle (°)	ζ potential (mV)	Water uptake (%)
0	96	3.82	24
0.01	86	-1.92	35
0.05	81	-4.94	40
0.1	74	-7.64	44
0.5	67	-12.46	48
1	63	-14.42	50
5	61	-17.50	53

3.4. Membrane permeability and rejection

Several organic/inorganic nanocomposite NF membranes with different GO loadings were tested to examine the effect of GO loadings on the NF membrane performance and to find the optimal composition of the NF membrane. The tested GO loadings were 0.01, 0.05, 0.1, 0.5, 1, and 5% wt.%. As the amount of GO loadings increased, it was clearly observed with the naked eye that the membranes became darker. GOs are graphitic materials whose colors are black. Therefore, the darker color of the membrane indicates that the membrane contains more GOs. For all experiments, the ionic salt (NaCl) concentration in the feed water was fixed to 1 mM. An increasing PBI concentration in membrane casting solution, produced an increase in salt rejection from 73 to 86 % accompanied by a decrease in both permeability and specific flux which drop from 1.16 to 0.19 L/m^2 h bar and from 18 to 3 L/m^2 h, respectively (Table 2). These salt rejections are relatively low compared with commercially available PA membranes that typically show rejections in excess of 90 % for NaCl. The incorporation of GOs into the 4 wt.% PBI membranes increased water flux significantly with a slightly increased salt rejection as the GO loading increased from 0 wt.% to 0.1 wt.% (Table 3). The addition of GOs to the 4 wt.% PBI membrane increased specific flux from 10 L/m^2 h to 16 L/m^2 h and salt

rejection from 82 % to 86 %.

Recent studies have indicated that improvements in wetting of a membrane surface can be critical in improving the membranes water permeability [19]. The addition of GO suggested a incompact membrane structure with increased membrane surface charge and wettability. Thus, higher salt rejection and higher permeability may be attributed to GO. However, higher GO content (than 0.1 wt.%) caused a serious nanoparticle aggregation to result in the performances of GO/PBI membranes decline. When GO loading was 5 % (w/v), the permeate flux and salt rejection were 53 L/m^2 h and 15 %, respectively. In this case, too much GO in the DMAc solvent solution prevents the formation of dense PBI matrix. Consequently, relatively large pores between aggregated GOs are produced resulting in high permeate flux but poor separation. From these results, it can be concluded that the reasonable GO loadings in PBI matrix are in the range of 0.01–0.1 wt.%.

Table 2. Control membrane NF performance as a function of different PBI concentrations.

PBI concentration (wt.%)	Permeability (L/m^2 h bar)	Flux (L/m^2 h)	NaCl rejection (%)
2	1.16 ± 0.08	18 ± 0.7	73 ± 1.1
3	0.84 ± 0.10	13 ± 0.9	80 ± 0.9
4	0.64 ± 0.09	10 ± 0.4	82 ± 1.0
5	0.39 ± 0.11	6 ± 0.8	84 ± 0.8
6	0.19 ± 0.04	3 ± 0.5	86 ± 0.7

Table 3. Membrane performance as a function of different GOs loading at constant PBI concentration (4 wt.%).

GOs loading (wt.%)	Permeability (L/m^2 h bar)	Flux (L/m^2 h)	NaCl rejection (%)
0	0.64 ± 0.09	10 ± 0.4	82 ± 1.0
0.01	0.77 ± 0.08	12 ± 0.7	84 ± 1.1
0.05	0.90 ± 0.08	14 ± 1.2	85 ± 0.9
0.1	0.97 ± 0.07	16 ± 1.1	86 ± 0.7
0.5	1.23 ± 0.06	19 ± 1.0	60 ± 1.2
1	1.55 ± 0.06	24 ± 0.9	39 ± 0.9
5	3.41 ± 0.05	53 ± 0.8	15 ± 1.1

3.5. Chlorine tolerance

3.5.1. Fourier transform infrared (FTIR) spectroscopy

Figure 15 and 16 show the FTIR spectra of the commercial PA TFC membrane and PBI membrane exposed to chlorine solutions (500 mg/L for 24 h). As shown in Fig. 15(a), the peaks at 3444 cm^{-1}, indicating hydrogen bonded N–H stretch [39,40], were slightly reduced due to chlorine-exposure. These peak disappearances of chlorine-exposed membrane occurred by FAC, weakening the N–H bond stretch or substituting chlorine for hydrogen [41]. In Fig. 15(b), the amide II bends were lost by chlorine exposure in slightly different degrees. Note that wavenumbers of 1640 cm^{-1} and 1545 cm^{-1} indicate amide I (C=O) and amide II (N–H, N–C) mode, respectively [39]. However, the FTIR spectra of the PBI membrane did not show any peak disapperances. As shown in Figure 16, the absorption bands at 3450-3250 and 1640 cm^{-1}, assigned to the stretching vibration of the N-H groups C=N groups in the imidazole units [28], did not show any peak differences. FTIR spectra demonstrate that amide bends in polyamide were weakened by exposure to disinfectants, although only those functional group changes were not enough to clarify the performance or surface changes of the membrane.

(a)

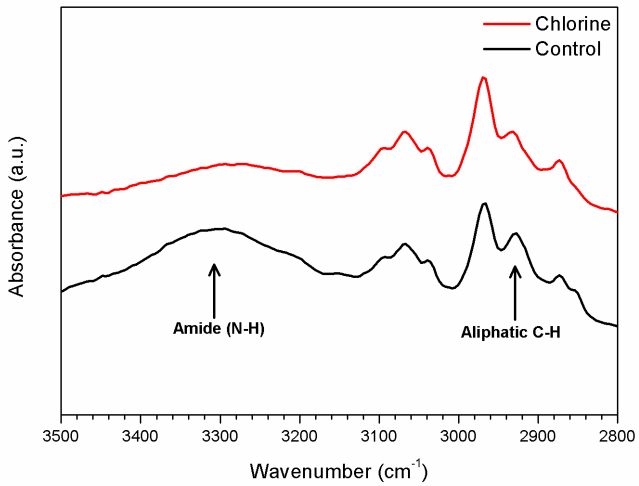

(b)

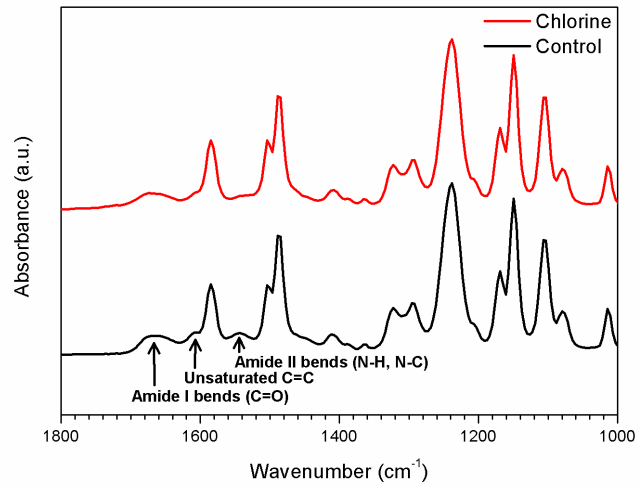

Fig. 15. FTIR absorption spectrum of chlorine-exposed commercial PA membrane (SWC5). Membrane were exposed in 500 mg/L for 24 h at pH 9.5 and 25 ℃. (a) The range of wavenumber is from 3500 cm^{-1} to 2800 cm^{-1} and (b) 1800 cm^{-1} to 1000 cm^{-1}.

(a)

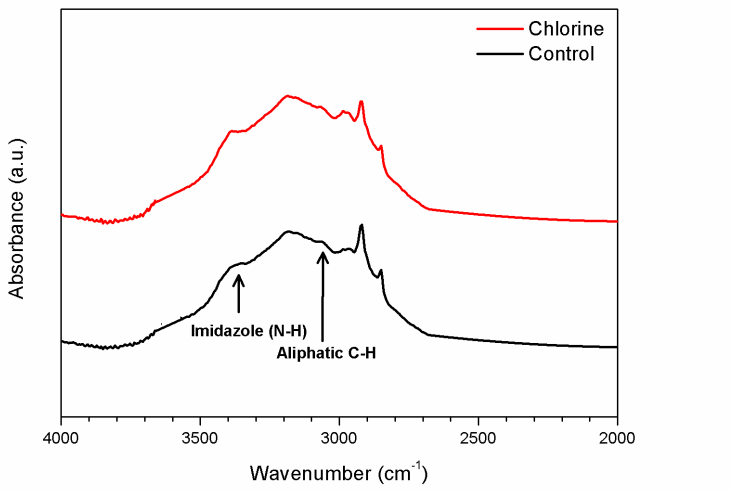

(b)

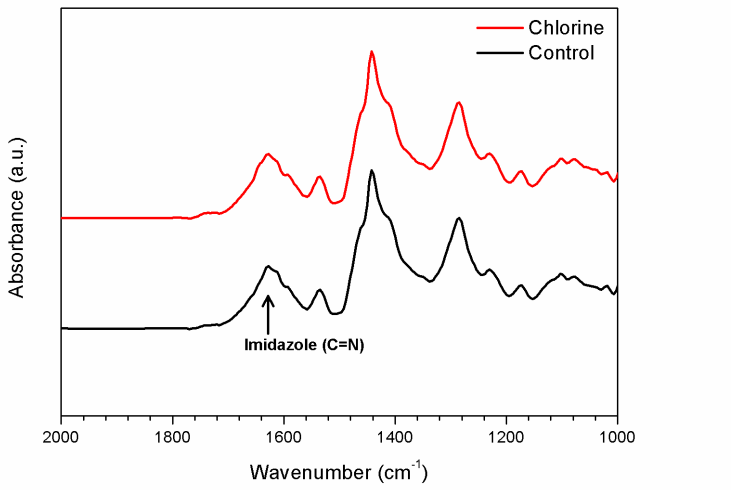

Fig. 16. FTIR absorption spectrum of chlorine-exposed PBI membrane. Membrane were exposed in 500 mg/L as TAC for 24 h at pH 9.5 and 25 ℃. (a) The range of wavenumber is from 3500 cm^{-1} to 2800 cm^{-1} and (b) 1800 cm^{-1} to 1000 cm^{-1}.

3.5.2. Effect of chlorine exposure time on membrane permeability and rejection

The membrane was exposed by a feed solution containing 1 mM NaCl and 500 ppm chlorine as NaOCl. After that, the membrane was operated in Dead-end filtration with a feed solution; the feed was buffered to pH 9.5. Figure 15 presents NaCl rejection and permeate flux as a function of chlorine exposure. The sample was pre-pared from 4 wt.% PBI solution. A commercial RO membrane (SWC5, Nitto Denko Hydranautics) was run for comparison. The NaCl rejection of the commercial PA membrane decreases by more than 20 % after only 10000 ppm-hours (20 h) of continuous exposure to chlorine and falls off even more rapidly thereafter. Such significant loss of salt rejection prohibits the use of chlorine for controlling biofouling in water being fed to such membranes without rigorous dechlorination to protect the membranes from chlorine exposure. In sharp contrast, there is no significant change in either NaCl rejection or water flux for the PBI membrane.

(a)

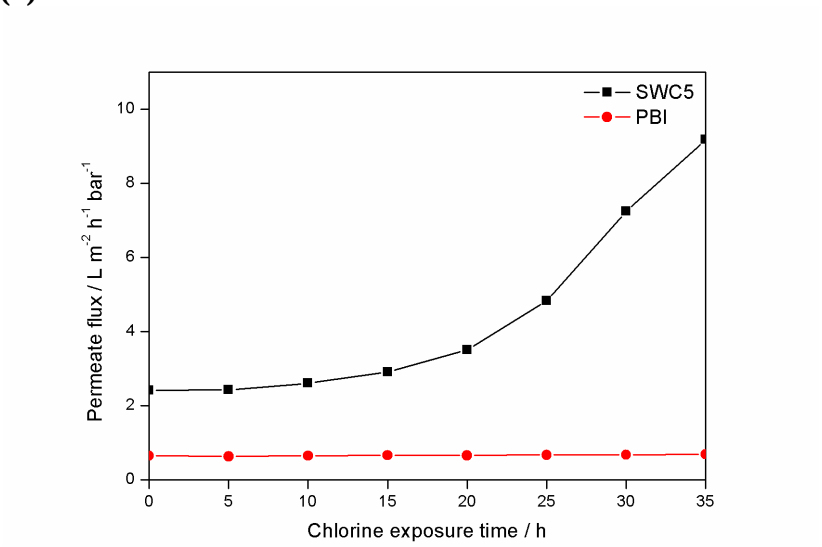

(b)

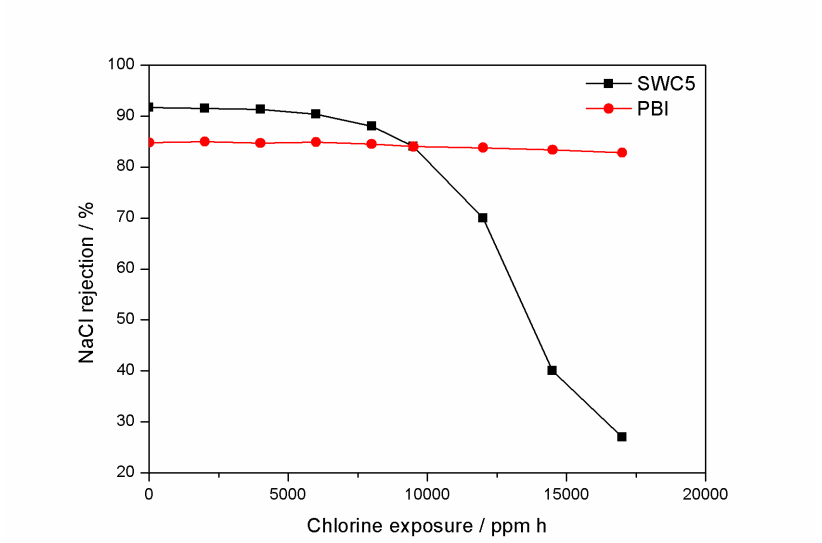

Figure 17. Effect of chlorine exposure on a) NaCl rejection and b) permeate flux of PBI thin film composite membrane and PA membrane (SWC5) at 25 ℃. Feed pressure 15.5 bar, feed composition 1 mM NaCl, dead end flow cell, pH 9.5, chlorine concentration = 500 ppm.

4. CONCLUSION

In summary, polybenzimidazole membranes, derived from the polycondensation reaction of 3,3-diaminobenzidine tetrahydrochloride and terephthalic acid using polyphosphoric acid as a solvent., exhibit high tolerance to chlorine over a wide pH range. Given their high chlorine tolerance, these membranes offer the possibility of desalinating and purifying water without the dechlorination steps that are now used before water is fed to membrane desalination units. The overall lower mass transport across the virgin membrane was believed to be due to the membranes higher hydrophobicity. The GO/PBI composite membranes were more hydrophilic than the pristine membrane. the more hydrophilic surface should unergo an increased wetting effect, where the membrane-fluid interactions favored water transport. In addition to the effect of the more hydrophilic surfaces, the charged membrane surfaces showed a higher degree of sodium chloride rejection. The results of introducing GO in the PBI membrane with the intent to increase hydrophilicity, wettability and surface charge show enhanced membrane performance both with respect to water flux and salt rejection. The results of Further studies are aimed at optimizing polymer design by employing cross-linked structures [42] and

sulfonated polymers [43] to simultaneously achieve high water permeability and high salt rejection while maintaining excellent chlorine tolerance.

5. References

1. Robert F. Service, *Desalination Freshens Up*. Science, 2006, 313, 1088-1090.
2. A.A. Burbano, S.S. Adham, W.R. Pearce, *The state of full scale RO/NF desalination results from a worldwide survey.* Journal AWWA, 2007, 99, 116-127.
3. R.J. Petersen, *Composite reverse osmosis and nanofiltration membranes*. Journal of membrane science, 1993, 83, 81-150.
4. E.T. Reese, M. Mandels, *Enzymatic degradation.* Cellulose and Cellulose Derivatives, edited by N M Bikales & L Segal (Wiley Interscience, New York) 1971, 1079-1094.
5. J.E. Cadotte, *Interfacially synthesized reverse osmosis membrane*. US Patent, 4,277,344, 1981.
6. T. Knoell, *Municipal wastewater: chlorine's impact on the performance and properties of polyamide membranes*. Ultrapure Water, 2006, 23, 24-31.
7. M.J. Hammer, M J. Hammer Jr., *Water Quality.* Water and Wastewater Technology, Prentice-Hall, Upper Saddle River, 2004, 249-251.
8. A.R. Pitochelli, E.L. Mainz, D.B. Griffith, *Biocides: useful applications for the use of Chlorine dioxide in water treatment*, Ultrapure Water 2006, 22(4), 40, 42-43.
9. R.J. Petersen, J.E. Cadotte in *Handbook of Industrial Membrane Technology* (Ed.: M.C. Porter), Noyes, ParkRidge, 1996, 307-348.
10. N.P. Isaias, *Experience in reverse osmosis pretreatment.* Desalination 2001, 139, 57-64.
11. J.A. Redondo, *Brackish, sea and wastewater desalination*. Desalination 2001, 138, 29-40.

12. M.B. Gieselman, J.R. Reynolds, *Water soluble polybenzimidazole based polyelectrolytes.* Macromolecules, 1992, 25, 4832-4834.
13. J. Davis Howard, W. Soehngen John, *Chlorine Resistant PBI RO Permselective Membranes.* Celanese research co summit N.J., 1981.
14. K.Y. Wang, T.S. Chung, J.J. Qin, *Polybenzimidazole (PBI) nanofiltration hollow fiber membranes applied in forward osmosis process.* Journal of Membrane Science, 2007, 300 6-12.
15. J.L. Lv, K.Y. Wang, T.S. Chung, *Investigation of amphoteric polybenzimidazole (PBI) nanofiltration hollow fiber membrane for both cation and anions removal*. Journal of Membrane Science, 2008, 310, 557–566.
16. K.Y. Wang, Y. Xiao, T.S. Chung, *Chemically modified polybenzimidazole nanofiltration membrane for the separation of electrolytes and cephalexin*. Chem. Eng. Sci., 2006, 61, 5807-5817.
17. M. Flanagan, R. Hausman, B. Digman, I.C. Escobar, M. Coleman, T.S. Chung, *Surface functionalization of polybenzimidazole membranes to increase hydrophilicity and charge.* Mod. Appl. Membr. Sci. Technol., 2011, 18, 303-321.
18. R. Hausman, B. Digman, I.C. Escobar, M. Coleman, T.S. Chung, *Functionalization of polybenzimidizole membranes to impart negative charge and hydrophilicity*. J. Membr. Sci. 2010, 363, 195-203.
19. J.R. McCutcheon, M. Elimelech, *Influence of membrane support layer hydrophobicity on water flux in osmotically driven membrane processes.* Journal of Membrane Science, 2008, 318, 458-466.
20. D.C. Marcano, et al., *Improved synthesis of graphene oxide*. ACS Nano, 2010, 4, 4806-4814
21. S. Stankovich et al, *Graphene based composite materials.* Nature, 2006, 442, 282-286.

22. T.H. Kim, T.W. Lim, J.C. Lee, *High-temperature fuel cell membranes based on mechanically stable para-ordered polybenzimidazole prepared by direct casting*, Journal of power sources 2007, 172, 172-179.

23. L. Xiao, H. Zhang, T. Jana, E. Scanlon, R. Chen, E.-W. Choe, L.S. Ramanathan, S. Yu, B.C. Benicewicz, *Synthesis and Characterization of Pyridine-Based Polybenzimidazoles for High Temperature Polymer Electrolyte Membrane Fuel Cell Applications*. Fuel Cells, 2005, 5, 287–295.

24. M. Hirata, T. Gotou, S. Horiuchi, M. Fujiwara, M. Ohba, *Thin film particles of graphite oxide 1: high-yield synthesis and flexibility of the particles.* Carbon, 2004, 42, 2929-2937

25. H.A. Becerril, J. Mao, Z. Liu, R.M. Stoltenberg, Z. Bao, Y. Chen, *Evaluation of solution processed reduced graphene oxide films as transparent conductors.* Acs Nano, 2008, 2, 463-470.

26. W. Shan, P. Bacchin, P. Aimar, M. Bruening, V. Tarabara, *Polyelectrolyte multilayer films as backflushable nanofiltration membranes with tunable hydrophilicity and surface charge*. Journal of membrane science, 2010, 209, 268-278.

27. J.A Osaheni, S.A Jenekhe, *Synthesis and Processing of Heterocyclic Polymers as Electronic, Optoelectronic, and Nonlinear Optical Materials. 4. New Conjugated Rigid-Rod Poly(benzobis(imidazole))s*. Macromolecules 1995, 28, 1172–1179.

28. S.K. Kim, T.H. Kim, J.W. Jung, J.C. Lee, *Polybenzimidazole containing benzimidazole side groups for high temperature fuel cell applications.* Polymer 2009, 50, 3495-3502.

29. T.T.P. Cheung, *X-ray photoemission of carbon: Lineshape analysis and application to studies of coals*, J. Appl. Phys 1982, 53, 6857-6862.

30. H.A. Katzman, P.M. Adams, T.D. Le and C.S. Hemminger, *Characterization of low thermal conductivity PAN-based carbon fibers.* Carbon, 1994, 32, 379-391.

31. E. Desimoni, G.I. Casella and A.M. Salvi, *XPS/XAES study of carbon fibres during thermal annealing under UHV conditions*. Carbon, 1992, 30, 521-526.

32. E. Papirer, R. Lacroix, J.B. Donnet, G. Nanse and P. Fioux, *XPS Study of the halogenation of carbon black-part 1. Bromination.* Carbon, 1994, 32, 1341-1358.

33. E. Desimoni, G.I. Casella, A. Morone and A.M. Salvi, *XPS determination of oxygen-containing functional groups on carbon-fibre surfaces and the cleaning of these surfaces*. Surf. Interface Anal., 1990, 15, 627-634.

34. Y. Xu, H. Bai, G. Lu, C. Li, G. Shi, *Flexible graphene films via the filtration of water-soluble noncovalent functionalized graphene sheets.* J. Am. Chem. Soc. 2008, 130, 5856–5857.

35. S. Stankovich, R.D. Piner, S.T. Nguyen, R.S. Ruoff, *Synthesis and exfoliation of isocyanate-treated graphene oxide nanoplatelets*. Carbon, 2006, 44, 3342–3347.

36. A.B. Bourlinos, D. Gournis, D. Petridis, T. Szabó, A. Szeri, I. Dékány, *Graphite oxide: chemical reduction to graphite and surface modification with primary aliphatic amines and amino acids*. Langmuir, 2003, 19, 6050–6055.

37. T.S. Chung, *A critical review of polybenzimidazoles: historical development and future R&D.* J. Macromol. Sci., Part C, Rev. Macromol. Chem. 1997, 37, 277-301.

38. N.W. Brooks, R.A. Duckett, J. Rose, I.M. Ward, *An nmr study of absorbed water in polybenzimidazole***,** Polymer, 1993, 34, 4038-4042.

39. D.J. Skrovanek, S.E. Howe, P.C. Painter, M.M. Coleman, *Hydrogen bonding in polymers: infrared temperature studies of an amorphous polyamide*. Macromolecules, 1985, 18, 1676-1683.

40. J.H. Yu, Y.B. Baek, H.S. Yoon, J.Y. Yoon, *New disinfectant to control biofouling of polyamide reverse osmosis membrane.* Journal of membrane science, 2013, 427, 30-36.

41. G. Kang, C. Gao, W. Chen, X. Jie, Y. Cao, Q. Yuan, *Study on hypochlorite degradation of aromatic polyamide reverse osmosis membrane*. Journal of membrane science, 2007, 300, 165-171.

42. S.K. Kim, S.W. Choi, W.S. Jeon, J.O. Park, T.Y. Ko, H. Chang, J.C. Lee, *Cross-Linked Benzoxazine Benzimidazole Copolymer Electrolyte Membranes for Fuel Cells at Elevated Temperature.* Macromolecules, 2012, 45, 1438-1446.

43. J.A. Mader, B.C. Benicewicz, *Sulfonated polybenzimidazoles for high temperature PEM fuel cells.* Macromolecules, 2010, 43, 6706-6715.

초 록

폴리아마이드 분리막은 제조단가가 낮고 분리막으로써 뛰어난 성능을 보여왔기 때문에 가장 보편적으로 수처리 공정을 진행하는데 사용되어져 왔으나, 화학적 안정성이 떨어져 염소이온 및 산화제에 쉽게 고분자 구조가 파괴되어 성능이 떨어지는 문제점을 보여왔다. 본 연구에서는, 기존 수처리 분리막의 단점을 극복하기 위해 폴리벤지미다졸을 합성하여 나노여과 수처리 분리막을 제조하였으며 폴리벤지미다졸 수처리 분리막이 현재 상용화 되어있는 폴리아마이드 역삼투 분리막 대비 뛰어난 화학적 안정성과 내염소성 특성을 보이는 것을 확인하였다. 폴리벤지미다졸 여과막의 낮은 투수율과 염제거율을 향상시키기 위해 산화그래핀을 폴리벤지미다졸 모재 내부에 분산시켜 복합막을 제조하는 실험을 추가로 진행하였으며 적외선 분광법 (FT-IR), X 선 광전자 분광법 (XPS), 접촉각 측정, 제타전위측정 및 수분흡수율측정을 통하여 분리막의 조성 및 표면특성을 분석하였다. 산화그래핀을 첨가한 복합분리막의 표면전위와 친수성이 증가한 것을 확인하였으며, 투수율과 염제거율이 동시에 향상되는 것을 확인하였다.

주요어 : 담수화, 폴리벤지미다졸, 나노여과막, 나노복합막, 산화그래핀, 내염소성

학번 : 2011-23415